Diagnosing Hawaii's Recent Drought

J. K. EISCHEID,[a,b] M. P. HOERLING,[b] X.-W. QUAN,[a,b] AND H. F. DIAZ[c]

[a] *Cooperative Institute for Research in Environmental University of Colorado Boulder, CIRES, Boulder, Colorado*
[b] *NOAA/Physical Science Laboratory, Boulder, Colorado*
[c] *University of Hawai'i at Mānoa, Honolulu, Hawaii*

(Manuscript received 27 September 2021, in final form 11 March 2022)

ABSTRACT: Hawaii's recent drought is among the most severe on record. Wet-season (November–April) rainfall deficits during 2010–19 rank second lowest among consecutive 10-yr periods since 1900. Various lines of empirical and model evidence indicate a principal natural atmospheric cause for the low rainfall, mostly unrelated to either internal oceanic variability or external forcing. Empirical analysis reveals that traditional factors have favored wetness rather than drought in recent decades, including a cold phase of the Pacific decadal oscillation in sea surface temperatures (SSTs) and a weakened Aleutian low in atmospheric circulation. But correlations of Hawaiian rainfall with patterns of Pacific sea level pressure and SSTs that explained a majority of its variability during the twentieth century collapsed in the twenty-first century. Atmospheric model simulations indicate a forced decadal signal (2010–19 vs 1981–2000) of Aleutian low weakening, consistent with recent observed North Pacific circulation. However, model ensemble means do not generate reduced Hawaiian rainfall, indicating that neither oceanic boundary forcing nor a weakened Aleutian low caused recent low Hawaiian rainfall. Additional atmospheric model experiments explored the role of anthropogenic forcing. These reveal a strong sensitivity of Hawaiian rainfall to details of long-term SST change patterns. Under an assumption that anthropogenic forcing drives zonally uniform SST warming, Hawaiian rainfall declines, with a range of 3%–9% among three models. Under an assumption that anthropogenic forcing also increases the equatorial Pacific zonal SST gradient, Hawaiian rainfall increases 2%–6%. Large spread among ensemble members indicates that no forced signals are detectable.

KEYWORDS: Annual variations; Climate variability; Decadal variability

1. Introduction

There has been a well-documented decline in Hawaiian rainfall during the wet season of November through April over the past 10–20 years. A number of factors have contributed to the observed decline, including changes in the fraction of heavier rainfall quantiles (Chu et al. 2010; Timm et al. 2011; Norton et al. 2011), in teleconnections between Hawaiian rainfall and large-scale climate modes, such as El Niño–Southern Oscillation (ENSO) and the Pacific decadal oscillation (PDO), and in regional-scale Hadley cell subsidence (Chu 1995; Chu et al. 2010; Diaz and Giambelluca 2012; Longman et al. 2015; Frazier and Giambelluca 2017; Frazier et al. 2018; Timm et al. 2021), as well in a longer-term context related to secular changes in North Pacific sea level pressure (Diaz et al. 2016).

While the earlier studies indicated a significant relationship in the historical period between Hawaiian rainfall variability and ENSO at different time scales (Chu 1989; Chu and Chen 2005; Timm et al. 2011; Diaz and Giambelluca 2012), the strength of that association has waned over recent decades (Diaz and Giambelluca 2012; Timm et al. 2021; O'Connor et al. 2015). In addition, atmospheric circulation features over the North Pacific, often associated with ENSO variability, such as the Pacific–North American pattern (PNA) and the North Pacific Oscillation (NPO) have also shown recent changes in their association with Hawaiian rainfall (Frazier et al. 2018; Timm et al. 2021).

For much of Hawaii, the contribution of the heavier rainfall quantiles to the seasonal total is particularly high, with the upper quintile of daily precipitation contributing 40%–50% in some cases to the seasonal totals (Timm and Diaz 2009; Chu et al. 2010; Timm et al. 2011). Timm et al. (2021) illustrate how a recent decline in Kona lows producing heavy rain for Hawaii has contributed to the observed decline in wet season rainfall for the state.

Two Hawaiian region rainfall time series are shown in Fig. 1 to illustrate the character of the recent drought and place it into a modern historical context. Figure 1a is based on the gridded precipitation dataset from the Global Precipitation Climatology Center (GPCC; see section 2). The one in Fig. 1b was first documented by Frazier et al. (2016) and Frazier and Giambelluca (2017) and extends from the 1920/21 November–April season through the 2018/19 season. Both time series indicate little reprieve from the succession of dry years that began near the end of the twentieth century. Indeed, the first two decades of the new millennium are drier that any 20-yr period since the beginning of the instrumental record circa 1900, and the period of persistent low rainfall during 2010–19 ranks among the driest decade in the instrumental record.

Given the strong influence of climate drivers such as North Pacific sea level pressure (SLP), ENSO, and the PDO on the

Supplemental information related to this paper is available at the Journals Online website: https://doi.org/10.1175/JCLI-D-21-0754.s1.

Corresponding author: M. P. Hoerling, martin.hoerling@noaa.gov

DOI: 10.1175/JCLI-D-21-0754.1

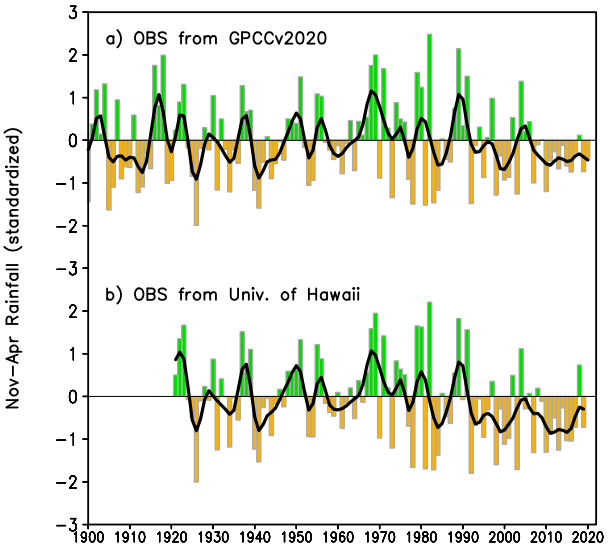

FIG. 1. Indices of observed November–April Hawaiian rainfall anomalies for (a) 1900–2020 (GPCC) and (b) 1920–2019 (University of Hawai'i). Anomalies are standardized on the basis of each dataset's available twentieth-century variability. Black curves are the smoothed time series based on a 9-point Gaussian filter. Raw interannual values of the two indices correlate at 0.96.

variability of Hawaiian rainfall, the relative constancy of below normal rainfall in recent years—while each of these indicators have varied considerably in the twenty-first century—is perhaps unexpected. In their detailed analysis of Hawaiian rainfall variability during 1920–2012 that included a focus on the long-term drying trend, Frazier et al. (2018) surmised that some recovery in Hawaiian rainfall was to be anticipated in response to the usual cycles of climate variability attending ENSO and PDO, and their related atmospheric structures of variability. This has yet to occur. Based on data studied through 2010 by Diaz and Giambelluca (2012), some of these modes had apparently lost their efficacy in driving Hawaiian rainfall in the twenty-first century. Indeed, they speculated on a possible change in the PDO–Hawaiian rainfall linkage, although the record was deemed too short to establish the significance of a change in what had hitherto been a strong historical correlation.

Here we update the period of analysis through 2020 to demonstrate that several key predictors for Hawaiian wintertime precipitation variability that have been identified in prior empirical analyses (e.g., Chu 1989; Diaz and Giambelluca 2012; Frazier et al. 2018; Timm et al. 2021) have largely failed to constrain island rainfall in the first two decades of the twenty-first century. This is in stark contrast to their strong linkages throughout most of the twentieth century and thus creates significant challenges for providing a physical explanation of the ongoing drought via reference to well-known modes of climate variability.

Our diagnosis of the Hawaiian drought then turns to assessing various possibilities for its nature and causes based on analysis of climate model experiments. For this purpose, we utilize atmospheric models performed in so-called AMIP (Atmospheric Model Intercomparison Project) mode (Gates et al. 1998) in which the historical variability of global sea surface temperatures and sea ice concentrations is specified. We conduct large ensembles of experiments to test whether the drought can be reconciled with the effects of boundary forcing in recent decades (i.e., a forced signal) versus whether its occurrence is best characterized as arising from purely unconstrained atmospheric variability (i.e., internal noise). This line of inquiry—using controlled model experiments—assesses whether Hawaii's protracted drought is indeed well described as a surprise event, as one might infer from the waning correlations on Hawaiian rainfall with the various aforementioned climate indicators. Such diagnostic methods have been extensively applied in prior studies on the nature and causes of regional droughts including oceanic origins for the North American Dust Bowl (e.g., Schubert et al. 2004; Seager et al. 2005), the U.S. Great Plains drought of 2012 (e.g., Hoerling et al. 2012), and the multiyear California drought of 2011–14 (Seager et al. 2015), to mention but a few. They have also been employed to assess the regional predictability of drought on seasonal to decadal time scales (Schubert et al. 2007). Here we use such methods to first diagnose whether decadal changes in oceanic forcing during recent decades as compared with those operating during the late twentieth century may account for development of the sustained regime of low Hawaiian rainfall.

A second line of diagnosis conducted herein—also using AMIP methods—will probe specifically whether longer-term trends in boundary forcings since the early twentieth century have materially affected the probability of low wintertime Hawaiian rainfall. Atmospheric model approaches have been previously used to explore analogous questions on how centennial-scale oceanic warming has affected risks for regional droughts (e.g., Hoerling and Kumar 2002, 2003; Hoerling et al. 2006; Schubert et al. 2007; Hoerling et al. 2010, 2012; Seager and Hoerling 2014). A strength of applying atmospheric modeling approaches to this problem is that the experiments are constrained by observed estimates of long-term sea surface temperatures (SST) warming patterns. The magnitude and structure of these observed changes can depart significantly from those simulated in historical coupled ocean–atmospheric models used in the Coupled Model Intercomparison Project (CMIP), yielding significant biases in regional climate change simulations that can adversely affect attribution of anthropogenic causes (e.g., Compo and Sardeshmukh 2009; Hoerling et al. 2012).

A challenge in interpreting AMIP approaches to diagnosing long-term change is that the attribution to human causes is uncertain barring a detection and attribution for the observed SST change itself. Here we will use two different estimates of observed long-term changes in SSTs to drive our model experiments, each of which has a line of evidence tying that boundary forcing to anthropogenic change as discussed further in section 2. Our purpose thereby is to probe how a diagnosis for recent low Hawaiian rainfall tied to anthropogenic forcing is robust to plausible but different observationally constrained assumptions of anthropogenic forcing. Section 2 presents datasets and methods including a detailed description

TABLE 1. Summary of the models and ensemble experiments used in this study.

Models	Expts	SST	Sea ice	Ensemble size
CAM5_100 km, L30	Hist 1980–2019	Obs 1980–2019	Obs 1980–2019	40
CAM5_25 km, L30	Hist 2009–19	Obs 2009–19	Obs 2009–19	10
	CFzm 2009–19	CFzm 2009–19	Avg 1979–89	5
	CF2d 2009–19	CF2d 2009–19	Avg 1979–89	5
ECHAM5_75 km, L30	Hist 1980–2019	Obs 1980–2019	Obs 1980–2019	50
	CFzm 2009–19	CFzm 2009–19	Avg 1979–89	50
	CF2d 2009–19	CF2d 2009–19	Avg 1979–89	50
FV3GFS_100 km, L64	Hist 1980–2019	Obs 1980–2019	Obs 1980–2019	20
	CFzm 2009–19	CFzm 2009–19	Avg 1979–89	20
	CF2d 2009–19	CF2d 2009–19	Avg 1979–89	20

of the model experiments. Results are presented in section 3, beginning with an examination of how to understand the current drought in a context of decadal variability and then in a context of centennial-scale change associated with global warming. A summary section 4 concludes with a synthesis of empirical and model results as to what we understand to be the causes for the current Hawaiian drought.

2. Data and methods

November–April rainfall for the Hawaiian Islands is extracted from the 0.25° Global Precipitation Climatology Center land–ocean gridded dataset (Adler et al. 2003) using the version GPCCv2020 (Schneider et al. 2020) for the 1900–2019 period. The gridded values were averaged together to develop the Hawaiian rainfall index (HRI) time series shown Fig. 1a. A station-based HRI time series (Frazier et al. 2016; Frazier and Giambelluca 2017; Lucas et al. 2022) is also used that spans the period 1920–2019. It is very similar to the GPCC version, with a correlation of 0.97 for the post-1950 period.

Atmospheric circulation and precipitation data are obtained from the 0.25° monthly gridded ERA5 reanalyses (Hersbach et al. 2020). Satellite-estimated precipitation analyses over

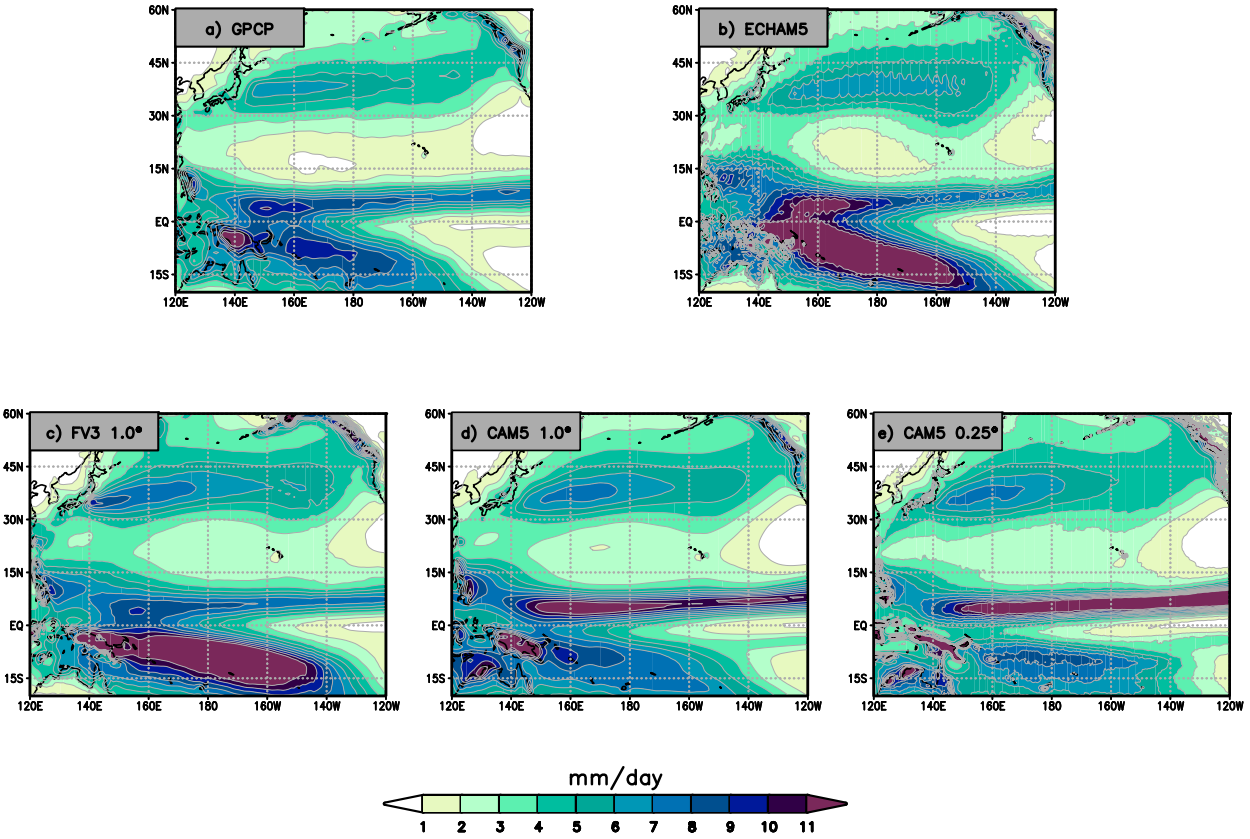

FIG. 2. Climatological November–April precipitation (mm day^{-1}) based on (a) GPCP satellite estimates, (b) ECHAM5 simulations, (c) FV3/GFS simulations, and (d),(e) CAM5 model simulations conducted at two different dynamical core resolutions. The period is 2010–19.

ocean regions is based on the Global Precipitation Climatology Project (GPCP) monthly gridded data (Huffman et al. 2001). Historical reanalysis data products are based on the Twentieth Century Reanalysis version 3 (Slivinski et al. 2019).

The climate model simulations used in this study are AMIP (Gates et al. 1998) style simulations in which the global atmospheric general circulation models are integrated with the prescribed evolution of observed global sea surface temperature and sea ice (SIC) as surface boundary forcing. Specific models and experiments used in this study are outlined in Table 1. The CAM5 (Neale et al. 2010) version used here is the atmospheric component of the Community Earth System Model version1 (CESM1) developed by the National Center of Atmospheric Research (NCAR). Ensemble experimental simulations are conducted with this model with two different horizontal resolutions of 100 and 25 km. The ECHAM5 model (Roeckner et al. 2003) is the fifth version of the atmospheric general circulation model by the Max Plank Institute for Meteorology developed for climate applications based primarily on a forecast model used by the European Centre for Medium-Range Weather Forecasts (ECMWF). Ensemble simulations with ECHAM5 are conducted with the horizontal resolution of 75 km and used here as an independent check to avoid biased attribution from a single model approach. The Global Forecast System (GFS) finite-volume cube sphere (FV3) model used herein is a version of the NOAA model currently employed for short-range numerical weather predictions (Bengtsson et al. 2019; Guan et al. 2022). Here we use a later version (v13.5) of the ensemble reforecast system (GEFSv12), and we conduct our experiments at a C96 scale (~1° horizontal resolution) rather than the C384 scale used in the reforecasts.

Two types of AMIP simulations are used. One is the conventional experiment noted here as *historical* (Hist) or *factual* simulations in which the models are integrated with boundary forcing specified with realistic temporal evolutions of SST, SIC, and radiative forcings. The monthly mean SST and SIC used here are from the product by Hurrell et al. (2008). Radiative forcings are specified with observed variations before the end of 2005 and the RCP6 scenario of CMIP5 (Taylor et al. 2012) thereafter. In general, these historical AMIP experiments realistically simulate the mean patterns of November–April precipitation including rainfall maximum in the North Pacific storm track, the tropical maximum in the ITCZ between 5° and 10°N and rainfall minima over the equatorial Pacific cold tongue and over the subtropical zonal band that includes the Hawaiian Islands and is dominated by the subsiding branch of the local Hadley cell (Fig. 2).

The second type of experiment is the so-called *counterfactual* AMIP simulations in which the long-term trends in SSTs, SIC, and atmospheric chemical composition since about 1900 are removed from the temporally evolving boundary conditions. In this study the estimated ocean warming pattern (i.e., the historical SST change) is calculated from the linear trend during 1900–2019 based on NOAA ERSSTv5 analyses. Here we use two estimates of the ocean warming pattern for driving the counterfactual simulations; one is the zonal average (CFzm) of SST trends (Fig. 3a) and the other is the more complicated two-dimensional pattern (CF2d) of SST trends

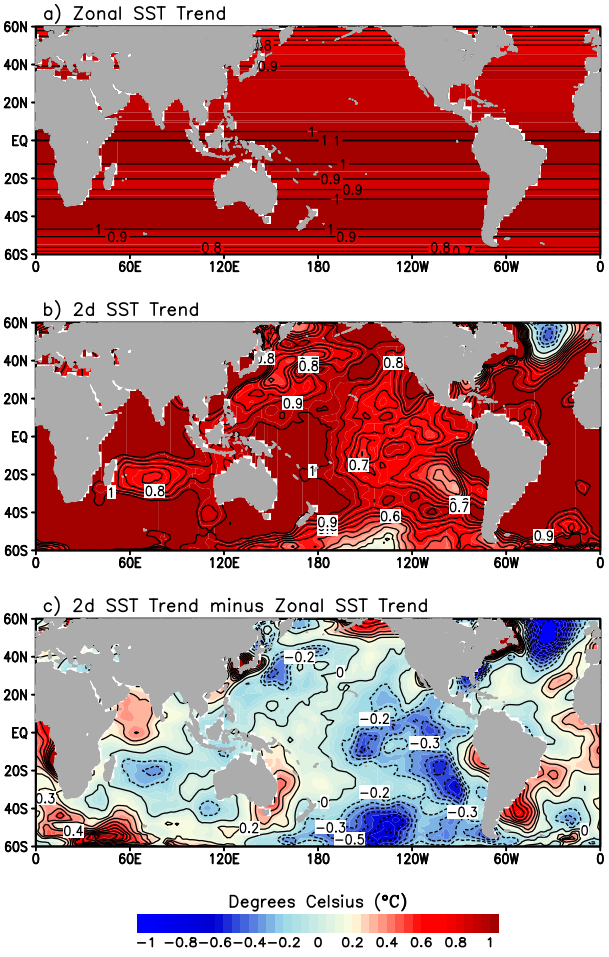

FIG. 3. Two estimates of the global warming patterns of historical SST change based on (a) zonally averaged trends for 1900–2019 and (b) the two-dimensional spatial pattern of SST trends for 1900–2019. Shown are the total changes over the 120-yr period. (c) The difference between their changes.

(Fig. 3b). The former can be argued to represent a more robust indication of anthropogenically forced SST changes than the full spatial pattern of SSTs given its detection and attribution to human-induced climate forcing (Knutson et al. 2013). The latter pattern (in particular the increase in the zonal gradient of SSTs across the equatorial Pacific), while having no formal attribution to anthropogenic forcing at this time, has been argued to represent a plausible transient evolution of tropical SSTs in response to global warming during the historical period (Heede and Fedorov 2021; Heede et al. 2021).

The delayed warming of the equatorial eastern Pacific relative to the remainder of the tropical oceans, although occurring in only a few of the CMIP6 models studied in Heede and Fedorov (2021), appears to arise from an oceanic thermostat effect together with anthropogenic aerosol induced cooling, both contributing to relatively fast transitory cooling responses of the tropical Pacific to global warming (Heede et al. 2021). While recognizing the qualitative nature of these new findings, and the possibility that some element of the observed two-dimensional trend

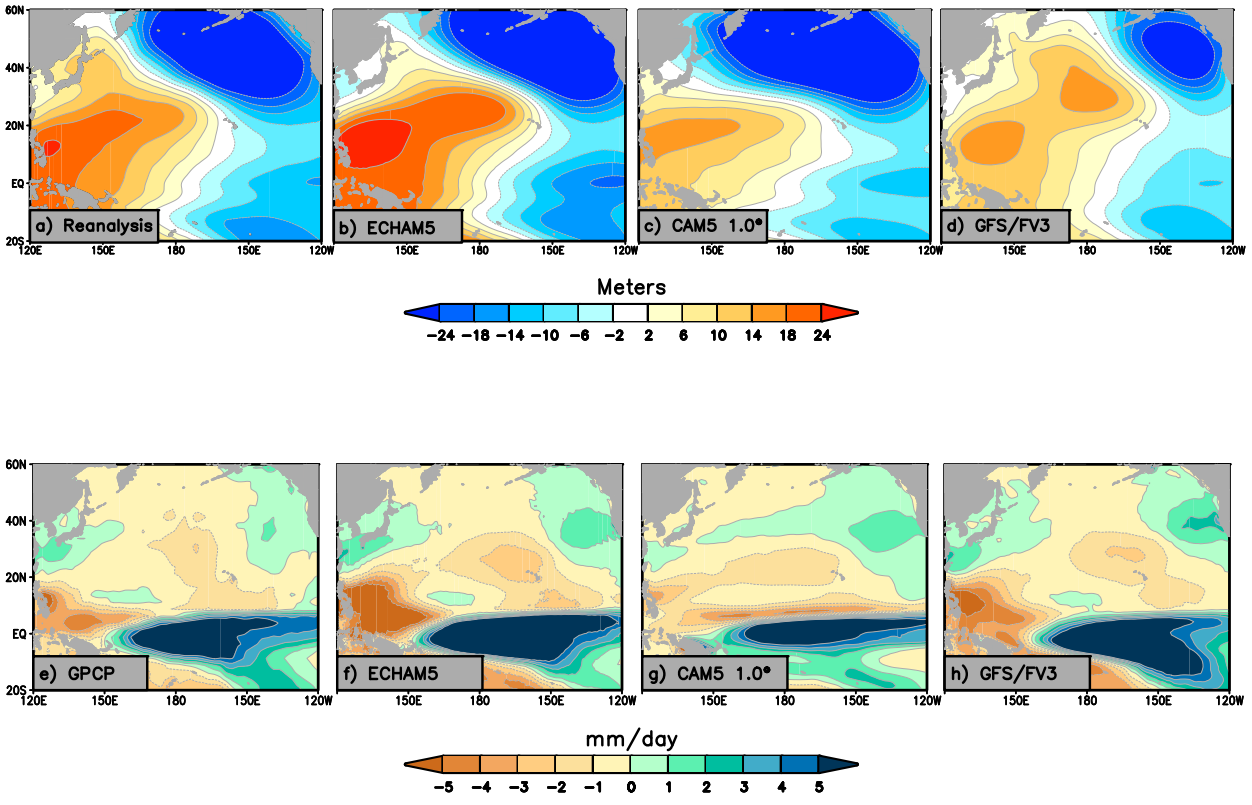

FIG. 4. (a),(e) Observed and model-simulated [(b),(f) ECHAM5; (c),(g) CAM5; (d),(h) GSF/FV3] November–April (top) 1000-hPa height anomalies (m) and (bottom) precipitation anomalies (mm day^{-1}) associated with the warm phase of El Niño–Southern Oscillation. Anomalies are the composite differences for eight El Niño (1983, 1987, 1992, 1998, 2010, 2015, 2016, and 2019) minus eight La Niña (1985, 1989, 1999, 2000, 2006, 2008, 2011, and 2018) events during 1979–2020.

pattern since 1900 likely also comingles internal decadal variability, we have conducted the additional suite of experiments using the more complicated historical trend pattern to assess the robustness of our model results to assumptions on the global ocean warming pattern. Figure 3c shows that the SST differences between these patterns is on the order of a few tenths of degrees Celsius but consists of a spatial pattern that resembles La Niña–like conditions to which Hawaiian rainfall is known to be sensitive.

The residual SST variability, after removing each of the trend patterns, is prescribed in the two sets of counterfactual simulations and thereby retains the major features of interannual and decadal SST variability (see also Sun et al. 2018). The adjustment to sea ice concentration is simply to replace the observed month-by-month variability with a repeating 1979–89 mean annual cycle, a period before appreciable decline in concentrations (e.g., Serreze and Stroeve 2015). Chemical composition including GHGs and anthropogenic aerosols are set to circa 1900 concentrations.

Two key attributes of the physics of Hawaiian rainfall variability are its links to atmospheric circulation variability and to ENSO-related SST variability. All three models simulate well the large-scale Pacific basin circulation patterns associated with their Hawaiian rainfall variability that captures the observed historical relationships (cf. Fig. S1 in the online supplemental material and Fig. 6a, described in more detail below). Concerning ENSO-related atmospheric sensitivity, Fig. 4 shows the November–April 1000-hPa height anomalies and precipitation anomalies associated with the warm phase of ENSO. Shown are composite differences between eight El Niño and eight La Niña events during 1979–2020. Each model provides a remarkably similar and realistic simulation of this particular, and verifiable, feature of tropical Pacific variability.

Based on these various indicators of simulated climatological means, teleconnections, and SST-forced sensitivities, the models are judged to be suitable for the study of decadal variability and climate change sensitivity to follow. We recognize, however, and caution that this evaluation is far from exhaustive of the attributes and biases of the various models employed herein especially as might pertain to the realism of their sensitivities to climate change driving. All the model and observational data used here are available for public access via the Facility for Weather and Climate Assessments (FACTS) data portal (Murray et al. 2020) hosted at NOAA's Physical Science Laboratory (PSL).

3. Results

a. *Empirical analysis of Hawaiian rainfall drivers*

Historical time series based on two different Hawaiian rainfall indices for November–April (Fig. 1) each reveal that the

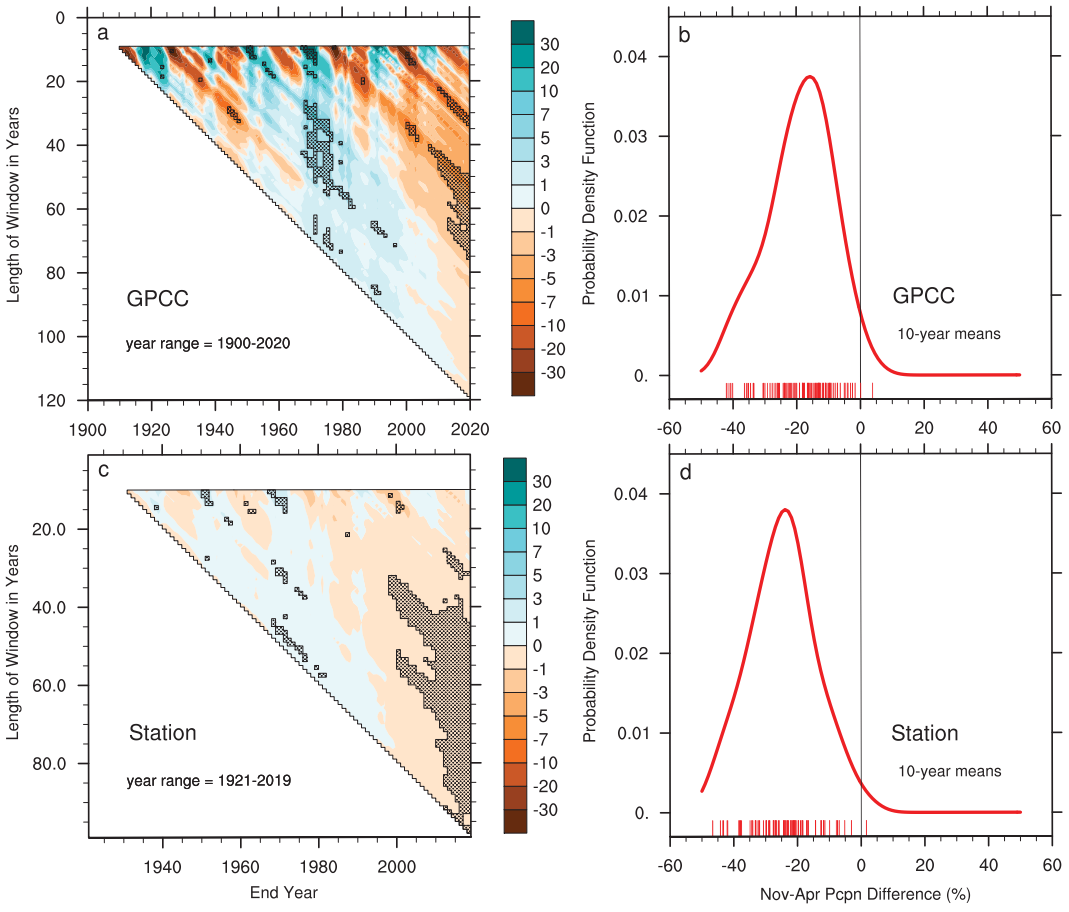

FIG. 5. Trend analysis of the GPCC-based Hawaiian rainfall index showing (a) rainfall trends for various segments beginning in 1900 and ending in 2020 and (b) a histogram of the 10-yr averaged Hawaiian rainfall anomaly (%) for 2010–19 calculated relative to all consecutive overlapping 10-yr periods during 1900–2009. (c),(d) As in (a) and (b), but for the trend analysis based on the University of Hawai'i estimated Hawaiian rainfall index that spans 1920–2019. For both Hawaiian rainfall indices, trends of November–April rainfall (mm yr^{-1}) are shown for all time segments of at least 10 years. Trends ending at the end of the data record are on the far-right side of the plot, with the longest trend segment shown at the bottom right. Periods of drying and wetting are shown in orange and green shades, respectively, and trends significant at 90% are stippled. The histogram curve is of the smoothed nonparametric probability distribution of the 110 or 90 samples for 2010–19 decadally averaged Hawaiian rainfall anomalies respectively based on the GPCC or University of Hawai'i index.

recent decades of dryness have been in stark contrast to an era of abundant precipitation during the 1960s to 1990s. Considerable decadal variability of Hawaiian rainfall throughout the record is evident. Whereas the University of Hawai'i HRI that begins in 1920 (bottom) indicates that the decades of the twenty-first century were the driest within its record, the longer GPCC HRI (top) indicates that a nearly comparable dry epoch occurred in the first decades of the twentieth century. Taken together, a simple narrative of Hawaiian low-frequency rainfall variability based on these time series is that the islands emerged from a dry period in the early twentieth century with increases peaking in the wet mid-twentieth century followed by a decline continuing into the early twenty-first century.

Trends in Hawaiian rainfall for all time segments of at least 10-yr duration are calculated using each HRI, the results of which are presented in Fig. 5. Statistically significant trends are hatched. Not surprisingly from inspection of Fig. 1, a drying trend exists for nearly all the time spans ending after about 2000: both indices yield statistically significant drying trends for segments beginning from the wet mid-twentieth century. A century-long drying trend (ending in 2019) is also statistically significant based on University of Hawai'i data. In contrast, owing to the presence of an antecedent dry era in the early twentieth century, a long-term drying trend spanning 120 years (ending in 2020) is not statistically significant in the GPCC data. That the recent period of dryness, although unusual for its persistence, is only modestly drier than during the early twentieth century is noteworthy and affirms the considerable natural multidecadal variability. Uncertainty in magnitudes of recent dryness among the two time series analyses

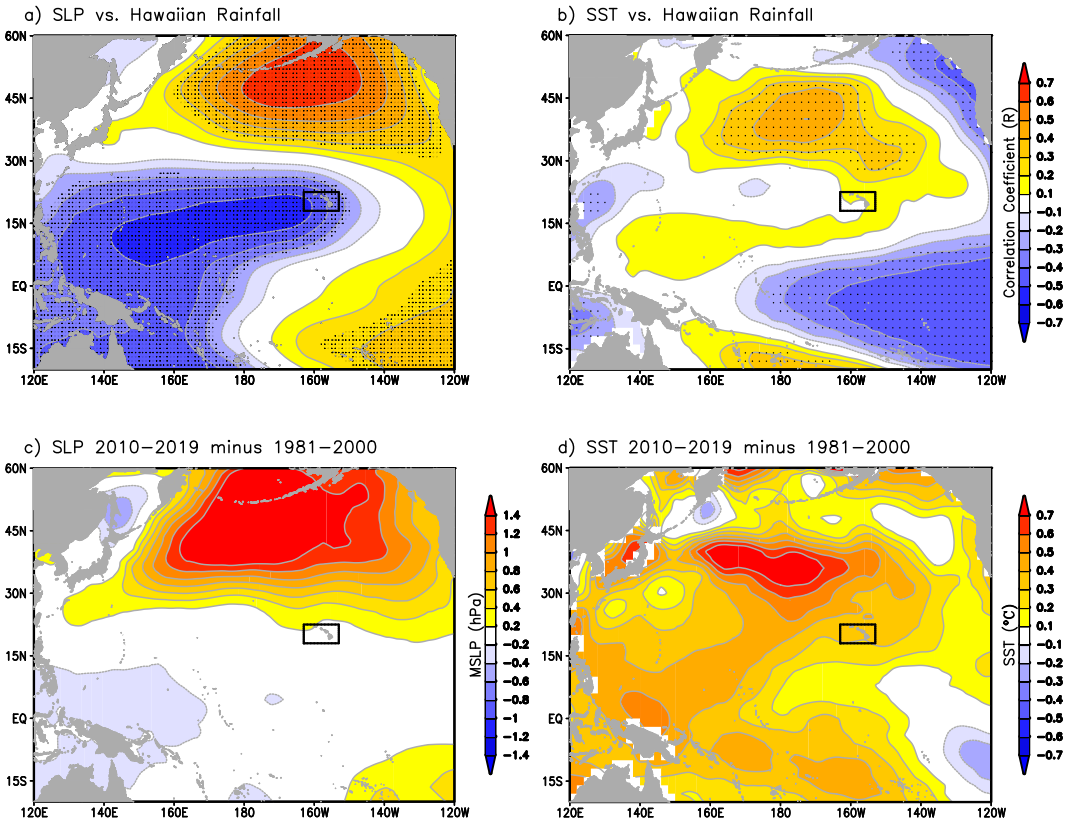

FIG. 6. The 1900–2000 correlations of the November–April GPCC Hawaiian rainfall index with (a) sea level pressure and (b) sea surface temperature. Also shown are 2010–19 November–April (c) sea level pressure anomalies (hPa) and (d) sea surface temperature anomalies (°C). Anomalies are relative to the 1981–2000 reference. Stippling indicates 95% significance based on Fisher's Z test. The black-outlined box indicates the Hawaiian region subsequently used to generate area-averaged model rainfall statistics (see Fig. 13, below). The area outlined is 18°–23°N, 163°–153°W.

must also be recognized. A consequence is that comparison of 1920–2019 trends yields statistically significant drying in the University of Hawai'i data but not in the GPCC data owing to more intense rainfall deficits analyzed in the former data post-2000 (see Fig. 1). These differences notwithstanding, it is clear that a treatment of the question of climate change is not readily amenable from this empirical data alone and will be deferred until section 3c in the context of model experiments.

Several patterns of Pacific basin climate variability have been empirically linked to wintertime Hawaiian rainfall during the twentieth century (e.g., Chu and Chen 2005; Diaz and Giambelluca 2012; Diaz et al. 2016; Frazier et al. 2018). One involves surface pressure, with Hawaii having been typically wet when high pressure prevailed over the Gulf of Alaska/Aleutian Islands in tandem with anomalously low pressure immediately west of Hawaii (Fig. 6a). The mechanism for the linkage involves a large-scale weakening of the subtropical trade winds and trade wind inversion, which are often favorable for island wetness overall. This meridional dipole pattern of sea level pressure resembles the west Pacific Oscillation of free atmospheric circulation (e.g., Barnston and Livezey 1987). These two centers tend to covary with the west–east fluctuations in the Pacific westerly jet. For instance, in the jets' retracted state, the pressure pattern often has the phase displayed in our Fig. 6 correlations, and moisture bearing subtropical low pressure systems (sometimes called Kona lows; see also Longman et al. 2021) more frequently affect Hawaii.

SST variations also correlate strongly with Hawaiian rainfall, particularly with those occurring over the far North Pacific and the tropical east Pacific. (Fig. 6b). These statistical relations depict, in part, an ocean forcing of the aforementioned SLP pressure patterns and in turn Hawaiian rainfall. The correlations also depict, especially over the extratropics, the ocean response to atmospheric forcing itself. During the twentieth century, statistically significant associations with Hawaiian rainfall are found with remote SST conditions over the North Pacific and the equatorial Pacific in a pattern that collectively resembles the Pacific decadal oscillation (PDO; Mantua et al. 1997). In its negative (cold) state, SSTs have the phase of the Fig. 6 correlations, and wintertime Hawaiian rainfall has tended to be above average. The PDO, however, is understood to involve a combination of different physical processes rather than a single basinwide coupled ocean–atmospheric mode (e.g., Newman et al. 2016). As such, not all aspects of the pressure and SST correlative centers of action of Fig. 6 need to be simultaneously present when Hawaiian rainfall is anomalous.

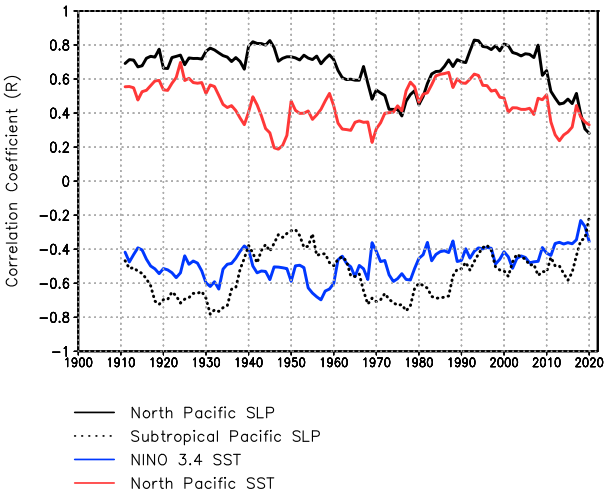

FIG. 7. 20-yr moving window correlations of November–April indices of extratropical North Pacific sea level pressure (solid black), subtropical North Pacific SLP (dotted black), North Pacific sea surface temperature (red), and Niño-3.4 (blue) with the GPCC Hawaiian rainfall index. The extratropical North Pacific SLP index is for the region 180°–150°W, 40°–60°N. The subtropical North Pacific SLP index is for 180°–160°W, 15°–25°N. The SST index is for the region 160°E–160°W, 30°–45°N. The Niño-3.4 is the index of SSTs averaged for the region 170°–120°W, 5°N–5°S. The period is 1900–2020, and the 20-yr correlation is plotted at the end point.

Further, the correlations are materially less than one, indicating that other processes are also associated with Hawaiian rainfall variability.

That processes other than those identified in Fig. 6a and 6b must also be important in causing Hawaiian rainfall variability is perhaps most clearly demonstrated when recognizing that recent dryness prevailed despite the presence of favorable large-scale Pacific climate conditions (Figs. 6c,d). A more rigorous treatment of the possible role of other factors is presented via modeling experiments in sections 3b and 3c. Suffice it here to note that the decadal atmosphere–ocean conditions over the tropical and North Pacific are quite reminiscent of those associated with wet Hawaiian winters prior to the recent drought, with strong high pressure anomalies over the Aleutian/Gulf of Alaska (Figs. 6a,c) and a Pacific basin SST pattern projecting on the cold phase of the PDO (Figs. 6b,d). Yet, dryness has been observed over the islands, indeed the driest such 20-yr period on record. Such an apparent incongruity of twenty-first-century climate conditions and Hawaiian rainfall has also been accompanied by a collapse in interannual correlations of winter rains with North Pacific SLP, subtropical Pacific SLP, North Pacific SSTs, and equatorial Pacific SSTs (Fig. 7). The historical strongest correlation, occasionally averaging above 0.8 in magnitude for moving 20-yr windows (Fig. 7, black curve), has been with Aleutian and subtropical North Pacific surface pressures. But for the 20-yr period of 2001–20 those surface pressure–related correlations have fallen below 0.3, their lowest values for any 20-yr period since 1900. While this recent weakening of the relation is extreme, a swift decline is not unprecedented—for instance, the 20-yr period 1956–75 also witnessed a sharp but brief decline in the North Pacific SLP–Hawaiian rainfall relationship.

In sum, the above empirically derived view is that Hawaii should have been wet, not dry, in recent decades based on large-scale atmospheric flow patterns, SST conditions, and their pre-2000 historical linkages with island winter rainfall. Interestingly, much of the subtropical Pacific in the latitude belt of the Hawaiian Islands has in fact been wet from about the date line to 150°W, in a manner that high Aleutian-region pressure and a cold ENSO-like Pacific oceanic condition would have historically dictated. Various reanalyses and satellite-derived estimates of the Pacific basin rainfall anomalies during 2010–19 (Fig. 8) give an impression of the recent Hawaiian drought as having been a "local" phenomenon—a further illustration of the island rainfall outwardly failing to conform to large-scale constraints. That the larger-scale rainfall was above normal during 2010–19 over much of the subtropical Pacific from the date line to 150°W does suggest that the teleconnection with various atmosphere–ocean modes of variability did not break down, on a larger spatial scale. There is ample empirical evidence of local rainfall indices experiencing appreciable decadal variability in their associations with patterns of climate variability (e.g., Diaz et al. 2001). However, it is reasonable to expect that if there were some underlying physical cause for changes in teleconnections, for instance linked to ENSO, that they would themselves have a large-scale articulation rather than consist of such a local flavor as manifest by the relative isolation of Hawaiian rainfall anomalies in Fig. 8.

b. Decadal forcing of the recent Hawaiian drought

Whereas the linear correlations between Hawaiian rainfall and indices of ENSO and the PDO weakened considerably in the twenty-first century, the possibility cannot be discounted that other ocean boundary forcing may have acted to provoke low rainfall and drought. To test that possibility, Fig. 9 presents the AMIP simulated decadal anomalies of 2010–19 relative to 1981–2000. It is over this roughly 40-yr period that a statistically significant reduction in Hawaiian rainfall was observed for both HRI time series (see Fig. 5). All three suites of ensemble model simulations indicate a forced decadal signal of North Pacific circulation change consisting of a weakened Aleutian low (Figs. 9a–d), broadly consistent with the observed weakening of the Aleutian low (left panel; shown are 1000-hPa height anomalies, which are very similar to those in SLP). The experiments thus affirm that this period of weakened Aleutian low pressure was appreciably boundary forced, although note that the magnitude of the ensemble mean simulated weakening is about one-half of that observed.

Nonetheless, neither of these three models generates a forced signal of reduced Hawaiian rainfall (Figs. 9e–h). Recall, from the observed empirical relationships of Fig. 7, that high Aleutian surface pressure is typically associated with wetter conditions over Hawaii. Similar empirical relationships are found in the models used herein (see Fig. S1 in the online supplemental material). It is therefore interesting to note, that despite the decadal signal of an extratropical circulation

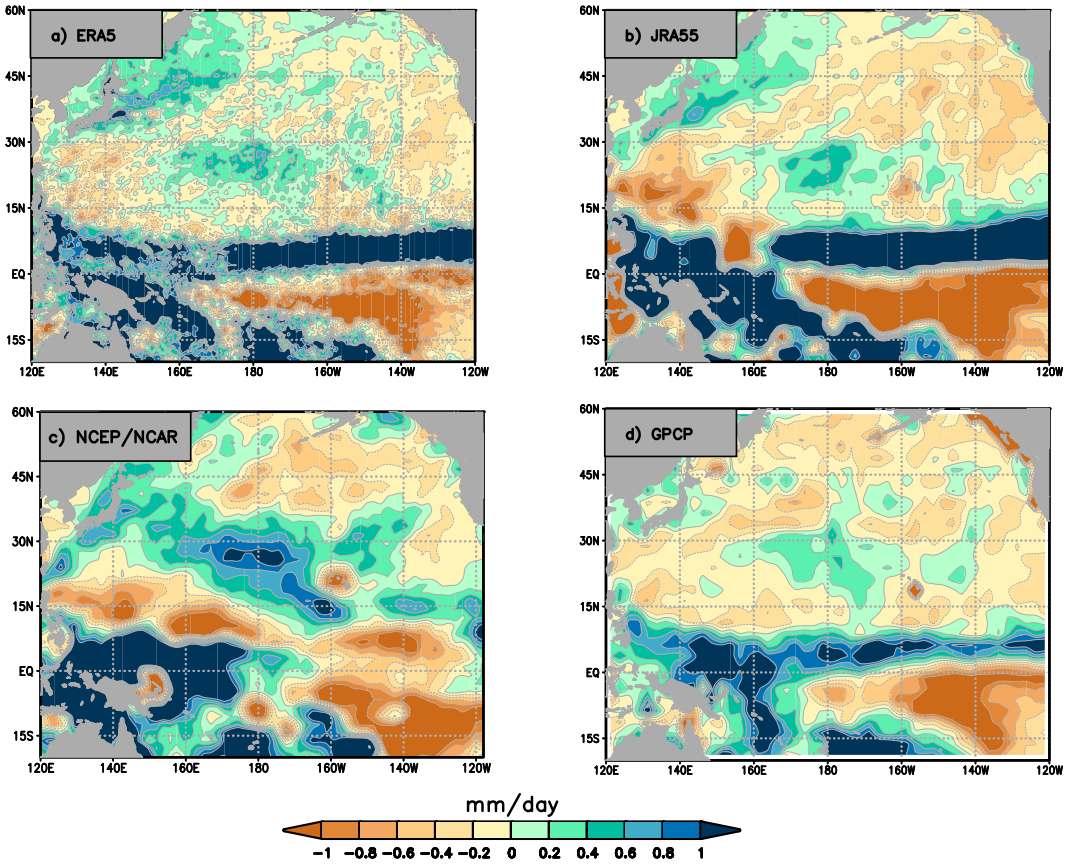

FIG. 8. Observed estimates of the 2010–19 November–April precipitation anomalies (mm day^{-1}) based on (a) ERA5, (b) JRA-55, (c) NCEP–NCAR reanalyses, and (d) satellite estimates (GPCP). The reference period is 1981–2000.

favorable for Hawaiian wetness in the simulations, the models yield no appreciable decadal wet signal. The principal area of wetness in the simulations resides west and north of the islands, not too dissimilar from the observed pattern (excepting the local dryness over Hawaii). Also, all three models generate an intensification of ITCZ convection between 5° and 10°N, with an attending drying near 10°–15°N. Such an ITCZ intensification is also evident in the decadal anomalies derived from the GPCP satellite product and in results derived from the ERA5 and JRA-55 reanalysis products (see Fig. 8). It is possible that these convection anomalies in the ITCZ have competed with decadal weakening of the Aleutian low, with Hawaii situated in a node between such competing wet and dry signals, although this is not an entirely satisfying explanation given the localized characteristic of the Hawaiian drought.

A further set of experiments using a fourth climate model (CAM6; see Fig. S2 in the online supplemental material), but having a smaller ensemble of 10 members, largely confirms the results of the models in Fig. 9. The forced decadal anomalies consist of Aleutian low weakening, a result in CAM6 that arises robustly whether controlled for the effects of tropical SST forcing only or using global boundary forcing. Again, the forced pattern of rainfall change does not include a reduction over the Hawaiian Islands, but a large-scale wettening mostly north and west of Hawaii.

c. *Climate change forcing of the recent Hawaiian drought*

The effect of centennial-scale climate change on Hawaiian rainfall during its severe drought decade is assessed using a parallel suite of atmospheric model simulations. In these, the climate of factual experiments subjected to the observed 2010–19 ocean boundary forcings and atmospheric chemical composition is contrasted with climate of that period absent effects of long-term global warming drivers—the counterfactual experiments (see section 2). Here we employ three models: CAM5 (at 0.25° spatial resolution), ECHAM5, and GFS/FV3. We also employ two different treatments of the long-term SST trend pattern, one that includes only the meridional pattern of zonally averaged SST trends for 1900–2019, and another that includes the full two-dimensional SST warming trend pattern.

For effects associated with observed zonal mean SST warming trends (and changes in atmospheric chemical composition), each model indicates a reduction in November–April Hawaiian rainfall in 2010–19 (Figs. 10d–f). In the case of ECHAM5 and GFS/FV3 simulations (Figs. 10d and 10f, respectively), the reasons for the drying are familiar—they

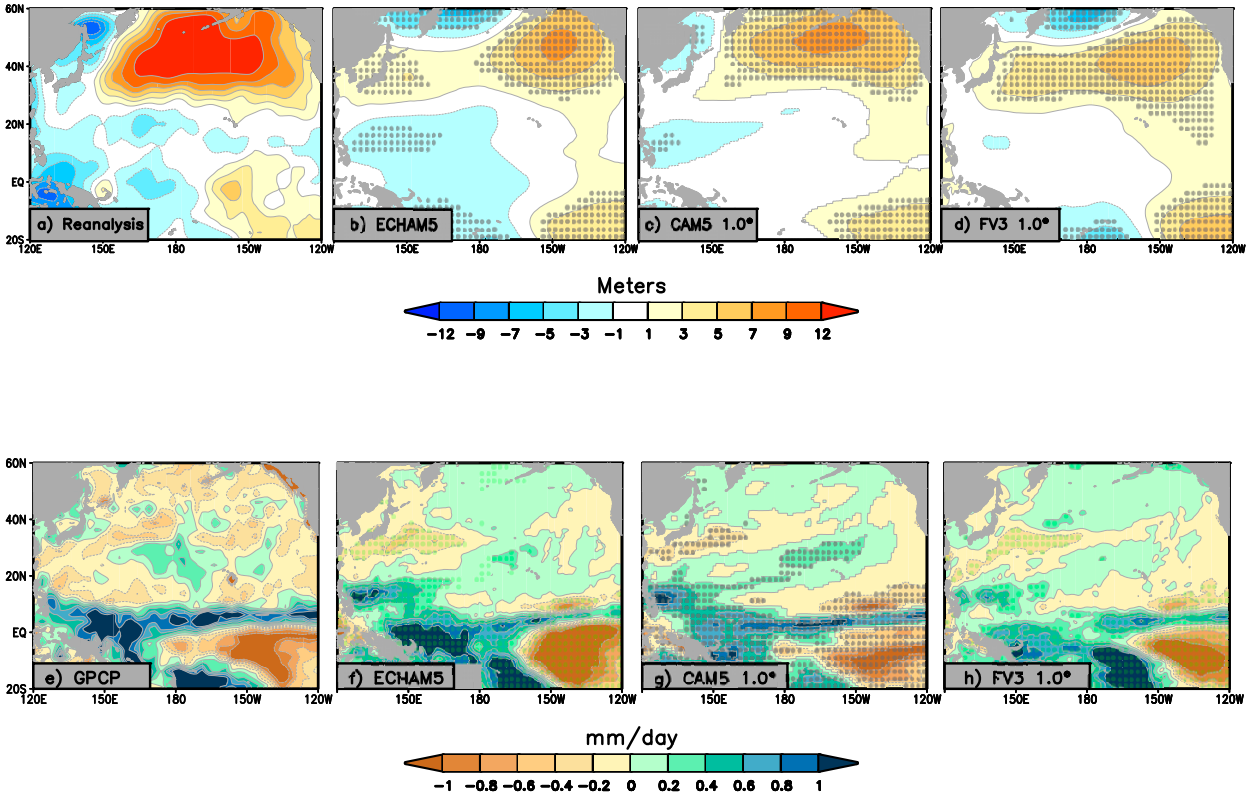

FIG. 9. (a),(e) Observed and model-simulated [(b),(f) ECHAM5; (c),(g) CAM5; (d),(h) GSF/FV3] November–April 1000-hPa (top) height anomalies (m) and (bottom) precipitation anomalies (mm day^{-1}) for 2010–19 relative to a 1981–2000 reference. Stippling indicates statistical significance at the 95% level.

are rooted in what we understand about interannual drivers of Hawaiian rainfall. The overall Pacific-wide precipitation response pattern in these models comprises North Pacific wetness and subtropical Pacific dryness that are linked with large-scale circulation changes. The latter consist of increased subtropical pressure immediately west of the islands and lower pressure over the Aleutians (Figs. 10a and 10c). Such a forced Pacific circulation change pattern and attending Hawaiian rainfall reduction mimics the empirical correlation structure occurring on interannual time scales (see Fig. 6), notwithstanding the fact that such linkage has waned in recent decades. In the case of CAM5, a nearly opposite phase of North Pacific circulation response occurs, in comparison with the other models with anomalous high pressure over the Aleutians (Fig. 10b). One might have expected, given this circulation pattern alone together with the correlation results of Fig. 6, wetter conditions over Hawaii in CAM5. But the rainfall declines instead (Fig. 10e). The spatial pattern of the Pacific basin rainfall anomalies in CAM5 reveals an intensified ITCZ band along 5°–10°N, which we speculate may be responsible for subsidence in the latitude band of Hawaii as suggested by the zonally extensive dry band across the subtropical Pacific. In sum, the indications are that while all three models produce Hawaiian-region drying in response to a zonally uniform ocean warming, the mechanisms in ECHAM5/GFS are likely different from those in CAM5.

For effects associated with the more complicated full spatial pattern of SST trends during 1900–2019, the models no longer indicate a decrease in Hawaiian rainfall (Figs. 11d–f). The simulated circulation patterns have only changed modestly in comparison with that arising from their sensitivity to zonal mean warming trends—but in important ways, as we address further below. Here we note again that the ECHAM5 and GFS/FV3 circulation responses are more similar to each other than to the CAM5. It might be tempting to judge the CAM5 response—a weakening of the Aleutian low—as the more realistic sensitivity given the similarity with observed anomalies of Fig. 9. But those were calculated as decadal variations over recent decades and are not directly comparable to these simulations of long-term change since 1900. Estimates of the observed long-term change in surface pressure based on different historical reanalysis products themselves differ considerably (not shown). Such analysis uncertainty, together with issues of detectability (addressed further below), limits confidence in rejecting either of these models' ensemble mean circulation responses. One should likewise be careful not to reject the CAM5 result merely on the basis that two other models agree with each other.

All three models do agree, however, in their Hawaiian rainfall sensitivity to the two different treatments of the SST warming trend pattern. The reasons for this switch in Hawaiian rainfall response from dry to wet is not immediately apparent

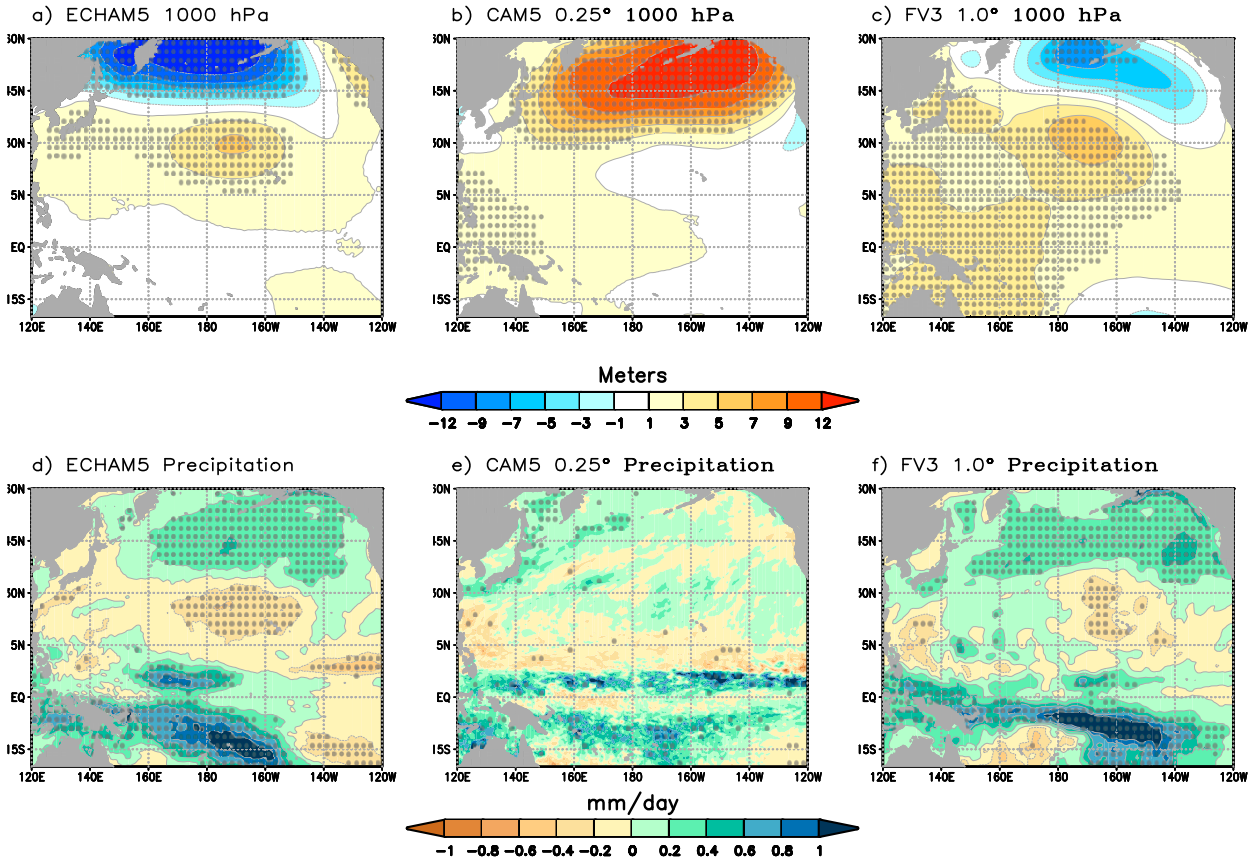

FIG. 10. The November–April 1000-hPa (a)–(c) height response (m) and (d)–(f) precipitation response (mm day^{-1}) to centennial-scale forcing based on the observed zonally averaged pattern of SST forcing change since 1900 for (left) ECHAM5, (center) CAM5 (0.25° resolution), and (right) FV3/GFS. Stippling indicates statistical significance at the 95% level.

from inspection of the circulation responses (Figs. 11a–c), which look very similar to those in the experiments based on the zonal-mean SST warming trends. The cause is the same in all three models, however, and lies in the Pacific basin's atmospheric sensitivity to rather subtle changes in zonal SST gradients. Recall from Fig. 3 that the two-dimensional pattern of SST trends consists of a strengthened equatorial Pacific zonal SST gradient of about 0.2°C. The effect of this (relative to a uniform SST warming)—which represents the atmospheric response to the SST differences of Fig. 3—is shown in Fig. 12. The circulation responses in all three models are similar and resemble the cold ENSO phase of teleconnection response pattern (i.e., the opposite polarity of anomalies shown in Fig. 4). The recovery of rainfall in the experiments using a long-term SST change forcing that consists of a strengthened equatorial Pacific SST gradient is thus qualitatively consist with the wet signal that each model generates over Hawaii in response to interannual La Niña conditions.

To close, we address two final questions: whether the simulated Hawaiian rainfall response to these two treatments of historical SST trends are statistically different, and whether either of these changes is likely to be detectable. Figure 13 presents histograms of the factual minus counterfactual 2010–19 Hawaiian region rainfall departures. All possible combinations of factual and counterfactual simulations are generated, yielding 2500, 50, and 400 samples for ECHAM5, CAM5, and GFS/FV3, respectively. The effect of observed zonally uniform SST was a 9%, 3%, and 7% decline in rainfall in ECHAM5, CAM5, and GFS/FV3, respectively. The spread of the histograms is greater than either of these models' signals with standard deviations among the individual model realizations greater than 10%. The signal-to-noise ratio is thus less than 1 for each model, indicative of low detectability. The effect of the more complicated two-dimensional SST warming trend pattern on Hawaiian region rainfall is even weaker and would thus be even less detectable—rainfall increases 6%, 2%, and 2% in ECHAM5, CAM5, and GFS/FV3, respectively. We do confirm, based on a Kolmogorov–Smirnov test applied to the histograms of Fig. 13, that the statistics of rainfall change in the two sets of experiments are different at a 90% or greater confidence level.

4. Discussion and summary

The aim of this study was to diagnose the principal climate factors operating on the Hawaiian Islands that led to a significant deficit in wet season (November–April) precipitation during the first decades of the twenty-first century. The period 2010–19 ranks among the driest decade for the Hawaiian

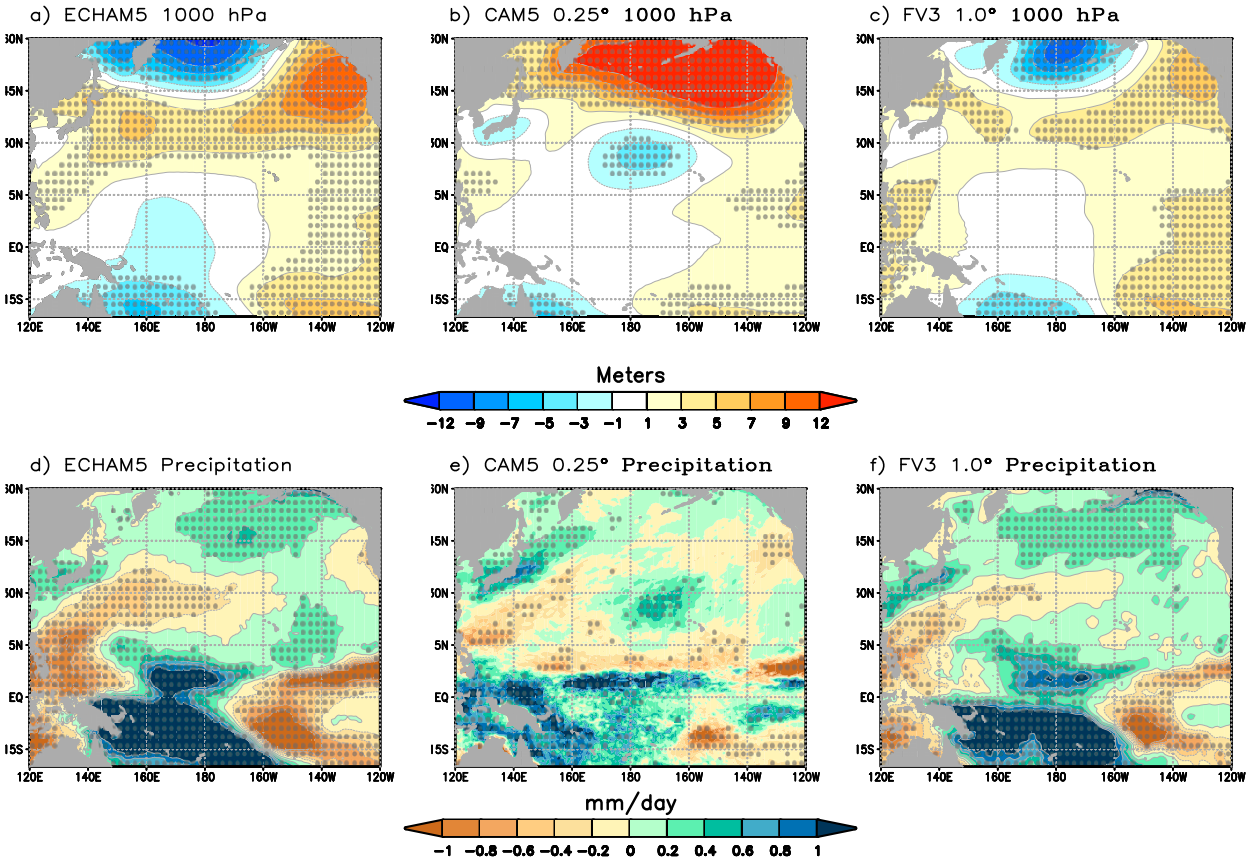

FIG. 11. As in Fig. 10, but based on using the observed two-dimensional pattern of SST forcing change since 1900.

Islands for any consecutive decade during the period since the turn of the twentieth century. Because a comparably dry decade occurred during the early twentieth century, the long-term trends of Hawaiian rainfall were found not to be statistically significant. However, statistically significant trends toward lower wintertime rainfall were found for segments beginning in the early 1980s (and ending in 2019/20) in part because of the prevailing wet conditions at that earlier time that stand in stark contrast to the low rainfall experienced in the early twenty-first century. Significant trends toward lower rainfall were also diagnosed for segments beginning in the mid-twentieth century, which likewise was a considerably wetter epoch in Hawaiian climate as inferred from two datasets studied herein.

Our empirically derived view is that Hawaii should have been wet, not dry, in recent decades. Both the large-scale observed atmospheric flow patterns and SST conditions were found to be favorable for wet conditions, at least when viewed through the lens of twentieth-century correlations. These included a weakened Aleutian low and a prevailing cold (negative) phase of the Pacific decadal oscillation describing the state of ocean conditions. Moving window correlations of Hawaiian rainfall with various Pacific climate indicators showed that strong associations in the twentieth century all but collapsed in the twenty-first century. Our results on a weakening of Hawaiian rainfall associations with Pacific basin patterns of climate variability are consistent with prior empirical studies (e.g., Diaz and Giambelluca 2012; Frazier et al. 2018; Timm et al. 2021). Such work suggests that a decline in relationships, as seen post-2000, may be an expression of interdecadal variability of Hawaiian rainfall with ENSO (e.g., Chu and Chen 2005; O'Connor et al. 2015), with the flavors of ENSO (Zhang et al 2020; Lu et al. 2020), and perhaps also with internal atmospheric decadal variability alone (e.g., Diaz et al. 2001). Our argument is for the latter process based on empirical considerations and subsequently confirmed by model experiments. A curious observed feature of the Hawaiian drought was its isolated character. Satellite and modern reanalysis products compel a characterization of the recent drought as a local phenomenon, with low Hawaiian rainfall embedded within a larger-scale pattern of high rainfall over much of the subtropical Pacific from the date line to 150°W. The empirical indicators thus implied the teleconnection with various atmosphere–ocean modes of variability did not break down, on a larger spatial scale, but perhaps only with indices of island rainfall itself. In this sense, the recent decadal Hawaiian drought stands in striking contrast to the comparably low Hawaiian rainfall decade of 1906–15. Then, a strong Aleutian low circulation prevailed (see Fig. S3 in the online supplemental material) outwardly explaining the drought in a fashion consistent with twentieth-century correlations. Now, a weak Aleutian low circulation and a cold phase of the PDO appear to be irreconcilable with the island drought event.

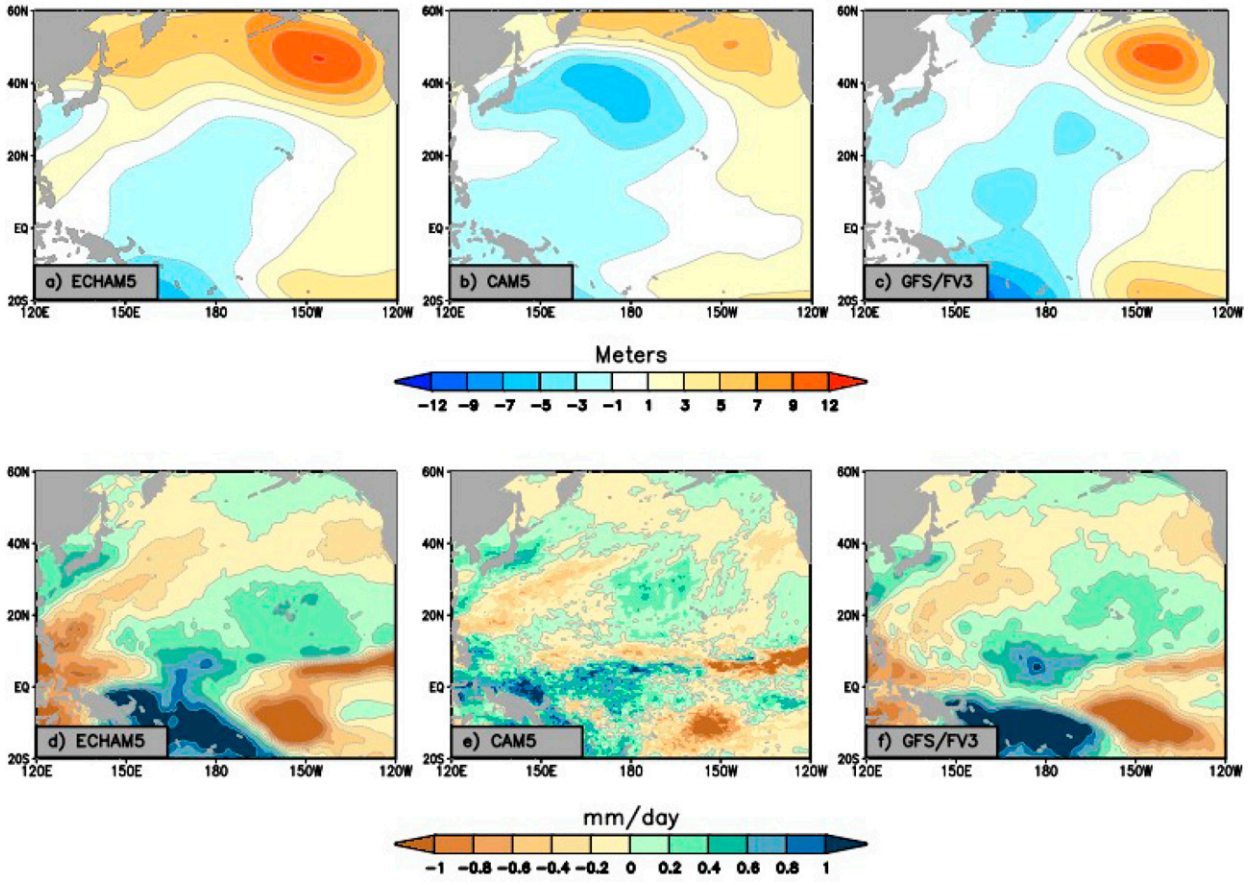

FIG. 12. The differences between simulated changes shown in Fig. 11 vs Fig. 10 for November–April (a)–(c) 1000-hPa heights (m) and (d)–(f) precipitation (mm day^{-1}). The anomalies represent the effects (in 2010–19) of differences in the two-dimensional SST trends relative to the zonally averaged SST trends of 1900–2019.

The empirical analysis raised at least as many questions as it answered, and the paper turned to climate model experiments to better understand what, if any, boundary forcings and associated large-scale climate drivers may have led to this prolonged period of dryness in Hawaii. They included several different ensemble AMIP simulations of the last decade (2010–19) in comparison with the late twentieth century, and a set of so-called event attribution simulations used to isolate the effect of long-term anthropogenic change forcing since the early twentieth century. Concerning decadal variability, four different models agree in revealing a forced signal of a weakened Aleutian low in the recent decade relative to the late twentieth century. However, neither of the model ensemble means yield reduced rainfall near and over the Hawaiian Islands. The absence of a signal and the large spread among members of the model simulations—each subjected to identical decadal boundary forcing variations—indicated that the recent decadal manifestation of Hawaiian drought was best reconcilable with internal atmospheric variability. These model results also support an argument that the anomalous circulation pattern in the North Pacific during the recent decade (the weakened Aleutian low) was unlikely responsible for the drought.

Additional model experiments explored how climate change since the early twentieth century may have affected Hawaiian rainfall in the early twenty-first century. Two different assumptions on the externally forced pattern of SST change, each derived from observed trends since 1900, were employed to address the sensitivity of Hawaiian region rainfall to plausible anthropogenic forcing. For a pattern of zonally uniform oceanic warming, the forced responses of three different atmospheric models all indicated drying, having a range of their signals from 3% to 9% declines. For a more complicated spatial pattern of SST warming that included an increase in the zonal contrast between the equatorial western and eastern Pacific, the forced responses of three different atmospheric models all indicated wettening, having a range of their signals from 2% to 6% increases. The origins for these different signals were traced to a La Niña–like teleconnection across the Pacific basin that captures the difference in responses to the two-dimensional versus zonally averaged ocean warming patterns.

The target of our analysis was rainfall over Hawaii, and its recent deficits. Beyond the empirical portion of our study that directly utilized indices of observed island rainfall, we relied extensively upon experiments with atmospheric models. It

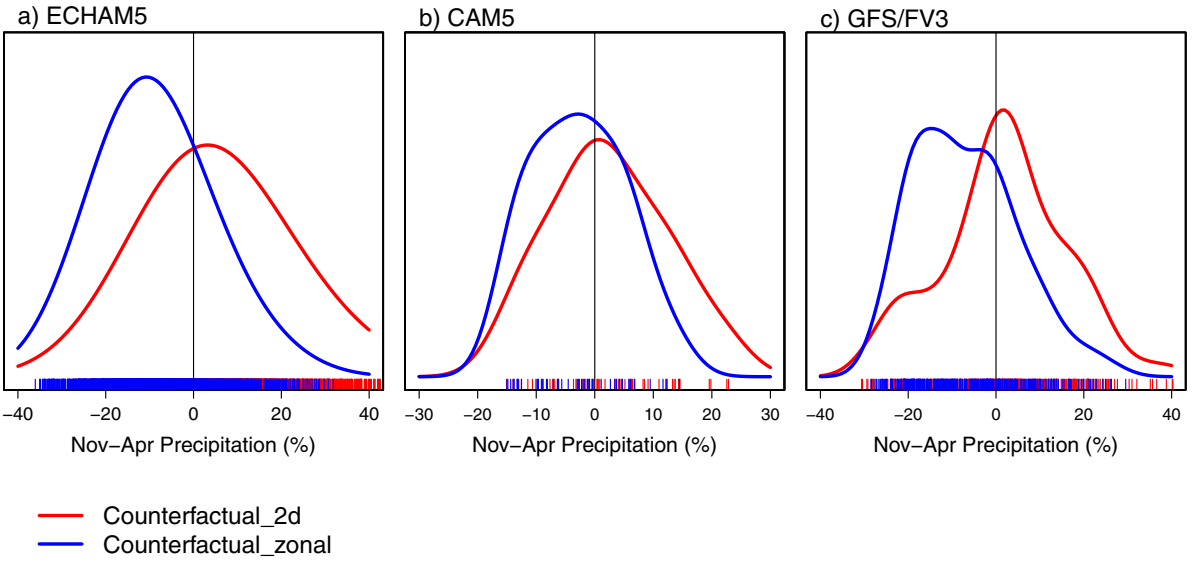

FIG. 13. Histograms of the November–April Hawaiian region precipitation responses (% change) to centennial-scale forcing based on the observed zonally averaged pattern of SST change since 1900 (blue curves) and the observed two-dimensional pattern of SST change since 1900 (red curves). Results are shown for (a) ECHAM5, (b) CAM5 (run at 0.25° resolution), and (c) GFS/FV3. Tic marks indicate individual samples of centennial change, consisting of 2500, 50, and 400 samples for ECHAM5, CAM5, and GFS/FV3, respectively. Mean Hawaiian region rainfall change is −9%, −2%, and −7% based on zonal mean change pattern of SST forcing in ECHAM5, CAM5, and GFS/FV3, respectively. Mean Hawaiian region rainfall change is +6%, +2%, and +2% based on two-dimensional change pattern of SST forcing in ECHAM5, CAM5, and GFS/FV3, respectively. The standard deviation among individual members for long-term Hawaiian precipitation change is 10%–14% for the models overall. The Hawaiian region used to generate area-averaged model rainfall statistics is 18°–23°N, 163°–153°W, shown in Fig. 6.

should be recognized that while these have spatial resolutions ranging from 25 to 100 km, which is adequate for many global and regional studies, the fidelity of rainfall simulations over the islands themselves is low given the complexity of terrain and small scales. We have demonstrated that each of the models used herein generates realistic climatological rainfall over the Pacific basin overall, and that the larger-scale associations between an index of Hawaiian-region rainfall with ENSO and also with patterns of Pacific-wide surface pressure variations are realistic in the three models used. Notwithstanding, it would be desirable to revisit the questions raised herein using higher-resolution regional climate models that can better resolve Hawaiian rainfall (see, e.g., Zhang et al. 2016a,b).

It should be kept in mind, based on our analysis of both observations and models, that significant decadal and centennial-scale variability in Hawaiian rainfall can arise without either internal oceanic boundary forcing or effects of external climate change drivers. Indeed, the fact that a comparably severe decade-long rainfall deficit affected Hawaii at the turn of the twentieth century suggests that external radiative forcing is not necessary. Given such empirical evidence for strong inherent variability of island rainfall, the model results are all the more plausible in their indications of a low signal-to-noise ratio of the simulated Hawaiian rainfall change for both treatments of the long-term SST change patterns.

Our results indicate that the direction in which climate change may have contributed to the twenty-first-century low wintertime Hawaiian rainfall depends on the assumption on how external radiative forcing acted to change sea surface temperatures, especially over the equatorial Pacific. It is beyond the scope of this study to determine which, if any, of these two patterns of long-term SST change is the more plausible fingerprint of global warming to date. Instead, it is perhaps more constructive to recognize that, for all the model precipitation change signals described above, their magnitudes are considerably less than their simulated internal variability of climate on centennial time scales (see also Quan et al. 2018). Recall that each ensemble member in our atmospheric model experiments experiences identical ocean boundary forcing and atmospheric chemical composition change, and as such the spread in histograms (e.g., Fig. 13) arises purely from internal atmospheric variability. It is perhaps surprising to see that atmospheric fluctuations alone, unconstrained by boundary forcing changes, could yield centennial-scale Hawaiian rainfall changes on the order of 20%. It is thus entirely possible to reconcile the observed severity of the recent Hawaiian decadal rainfall deficits with unforced internal variability alone.

Acknowledgments. We thank Andrew Hoell for helpful and constructive comments on earlier drafts of the paper and Thomas Giambelluca for providing the University of Hawai'i dataset. We also thank two anonymous reviewers for their comments on an earlier version of the paper.

Data availability statement. All of the monthly model data used in this study are available for public access via the

FACTS data repository (https://psl.noaa.gov/repository/facts/). In addition, the observed gridded data are available online (https://www.dwd.de/EN/ourservices/gpcc/gpcc.html). The observed station data for Hawaii were acquired from Dr. Thomas Giambelluca at the University of Hawai'i.

REFERENCES

Adler, R. F., and Coauthors, 2003: The version 2 Global Precipitation Climatology Project (GPCP) monthly precipitation analysis (1979–present). *J. Hydrometeor.*, **4**, 1147–1167, https://doi.org/10.1175/1525-7541(2003)004<1147:TVGPCP>2.0.CO;2.

Barnston, A. G., and R. E. Livezey, 1987: Classifications, seasonality, and persistence of low-frequency atmospheric circulation patterns. *Mon. Wea. Rev.*, **115**, 1083–1126, https://doi.org/10.1175/1520-0493(1987)115<1083:CSAPOL>2.0.CO;2.

Bengtsson, L., and Coauthors, 2019: Convectively coupled equatorial wave simulations using the ECMWF IFS and the NOAA GFS cumulus convection schemes in the NOAA GFS model. *Mon. Wea. Rev.*, **147**, 4005–4025, https://doi.org/10.1175/MWR-D-19-0195.1.

Chu, P.-S., 1989: Hawaiian drought and the Southern Oscillation, 1989. *Int. J. Climatol.*, **9**, 619–631, https://doi.org/10.1002/joc.3370090606.

——, 1995: Hawaii rainfall anomalies and El Niño. *J. Climate*, **8**, 1697–1703, https://doi.org/10.1175/1520-0442(1995)008<1697:HRAAEN>2.0.CO;2.

——, and H. Chen, 2005: Interannual and interdecadal rainfall variations in the Hawaiian Islands. *J. Climate*, **18**, 4796–4813, https://doi.org/10.1175/JCLI3578.1.

——, Y. R. Chen, and T. A. Schroeder, 2010: Changes in precipitation extremes in the Hawaiian Islands in a warming climate. *J. Climate*, **23**, 4881–4900, https://doi.org/10.1175/2010JCLI3484.1.

Compo, G. P., and P. D. Sardeshmukh, 2009: Oceanic influences on recent continental warming. *Climate Dyn.*, **32**, 333–342, https://doi.org/10.1007/s00382-008-0448-9.

Diaz, H. F., and T. W. Giambelluca, 2012: Changes in atmospheric circulation patterns associated with high and low rainfall regimes in the Hawaiian Islands region on multiple time scales. *Global Planet. Change*, **98–99**, 97–108, https://doi.org/10.1016/j.gloplacha.2012.08.011.

——, M. Hoerling, and J. Eischeid, 2001: ENSO variability, teleconnections, and climate change. *Int. J. Climatol.*, **21**, 1845–1862, https://doi.org/10.1002/joc.631.

——, E. R. Wahl, E. Zorita, T. W. Giambelluca, and J. K. Eischeid, 2016: A five-century reconstruction of Hawaiian Islands rainfall. *J. Climate*, **29**, 5661–5674, https://doi.org/10.1175/JCLI-D-15-0815.1.

Frazier, A. G., and T. W. Giambelluca, 2017: Spatial trend analysis of Hawaiian rainfall from 1920 to 2012. *Int. J. Climatol.*, **37**, 2522–2531, https://doi.org/10.1002/joc.4862.

——, ——, H. F. Diaz, and H. L. Needham, 2016: Comparison of geostatistical approaches to spatially interpolate month-year rainfall for the Hawaiian Islands. *Int. J. Climatol.*, **36**, 1459–1470, https://doi.org/10.1002/joc.4437.

——, O. E. Timm, T. W. Giambelluca, and H. F. Diaz, 2018: The influence of ENSO, PDO and PNA on secular rainfall variations in Hawai'i. *Climate Dyn.*, **51**, 2127–2140, https://doi.org/10.1007/s00382-017-4003-4.

Gates, W. L., and Coauthors, 1998: An overview of the results of the Atmospheric Model Intercomparison Project (AMIP-I). *Bull. Amer. Meteor. Soc.*, **73**, 1962–1970, https://doi.org/10.1175/1520-0477(1992)073<1962:ATAMIP>2.0.CO;2.

Guan, H., and Coauthors, 2022: GEFSv12 reforecast dataset for supporting subseasonal and hydrometerological applications. *Mon. Wea. Rev.*, **150**, 647–665, https://doi.org/10.1175/MWR-D-21-0245.1.

Heede, U. K., and A. V. Fedorov, 2021: Eastern equatorial Pacific warming delayed by aerosols and thermostat response to CO_2 increase. *Nat. Climate Change*, **11**, 696–703, https://doi.org/10.1038/s41558-021-01101-x.

——, ——, and N. Burls, 2021: A stronger versus weaker Walker circulation: Understanding model differences in fast and slow tropical Pacific responses to global warming. *Climate Dyn.*, **57**, 2505–2522, https://doi.org/10.1007/s00382-021-05818-5.

Hersbach, H., and Coauthors, 2020: The ERA5 global reanalysis. *Quart. J. Roy. Meteor. Soc.*, **146**, 1999–2049, https://doi.org/10.1002/qj.3803.

Hoerling, M., and A. Kumar, 2002: Atmospheric response patterns associated with tropical forcing. *J. Climate*, **15**, 2184–2203, https://doi.org/10.1175/1520-0442(2002)015<2184:ARPAWT>2.0.CO;2.

——, and ——, 2003: The perfect ocean for drought. *Science*, **299**, 691–694, https://doi.org/10.1126/science.1079053.

——, J. Hurrell, J. Eischeid, and A. Phillips, 2006: Detection and attribution of twentieth-century northern and southern African rainfall change. *J. Climate*, **19**, 3989–4008, https://doi.org/10.1175/JCLI3842.1.

——, J. Eischeid, and J. Perlwitz, 2010: Regional precipitation trends: Distinguishing natural variability from anthropogenic forcing. *J. Climate*, **23**, 2131–2145, https://doi.org/10.1175/2009JCLI3420.1.

——, ——, ——, X. Quan, T. Zhang, and P. Pegion, 2012: On the increased frequency of Mediterranean drought. *J. Climate*, **25**, 2146–2161, https://doi.org/10.1175/JCLI-D-11-00296.1.

Huffman, G., J. R. F. Adler, M. M. Morrissey, S. Curtis, R. Joyce, B. McGavock, and J. Susskind, 2001: Global precipitation at one-degree daily resolution from multi-satellite observations. *J. Hydrometeor.*, **2**, 36–50, https://doi.org/10.1175/1525-7541(2001)002<0036:GPAODD>2.0.CO;2.

Hurrell, J., J. Hack, D. Shea, J. Caron, and J. Rosinski, 2008: A new sea surface temperature and sea ice boundary dataset for the Community Atmosphere Model. *J. Climate*, **21**, 5145–5153, https://doi.org/10.1175/2008JCLI2292.1.

Knutson, T. R., F. Zeng, and A. Wittenberg, 2013: Multimodel assessment of regional surface, temperature trends: CMIP3 and CMIP5 twentieth century simulations. *J. Climate*, **26**, 8709–8743, https://doi.org/10.1175/JCLI-D-12-00567.1.

Longman, R. J., H. F. Diaz, and T. W. Giambelluca, 2015: Sustained increases in lower tropospheric subsidence over the central tropical North Pacific drives a decline in high elevation precipitation in Hawaii. *J. Climate*, **28**, 8743–8759, https://doi.org/10.1175/JCLI-D-15-0006.1.

——, O. E. Timm, T. W. Giambelluca, and L. Kaiser, 2021: A 20-year analysis of disturbance-driven rainfall on O'ahu, Hawai'i. *Mon. Wea. Rev.*, **149**, 1767–1783, https://doi.org/10.1175/MWR-D-20-0287.1.

Lu, B., P.-S. Chu, S.-H. Kim, and C. Karamperidou, 2020: Hawaiian regional climate variability during two types of El Niño. *J. Climate*, **33**, 9929–9943, https://doi.org/10.1175/JCLI-D-19-0985.1.

Lucas, M. P., R. J. Longman, T. W. Giambelluca, A. G. Frazier, J. McLean, S. B. Cleveland, Y.-F. Huang, and J. Lee, 2022: Optimizing automated kriging to improve spatial

interpolation of monthly rainfall over complex terrain. *J. Hydrometeor.*, **23**, 561–572, https://doi.org/10.1175/JHM-D-21-0171.1.

Mantua, N. J., S. R. Hare, Y. Zhang, J. M. Wallace, and R. C. Francis, 1997: A Pacific interdecadal climate oscillation with impacts on salmon production. *Bull. Amer. Meteor. Soc.*, **78**, 1069–1079, https://doi.org/10.1175/1520-0477(1997)078<1069:APICOW>2.0.CO;2.

Murray, D., and Coauthors, 2020: Facility for Weather and Climate Assessments (FACTS)—A community resource for assessing weather and climate variability. *Bull. Amer. Meteor. Soc.*, **101**, E1214–E1224, https://doi.org/10.1175/BAMS-D-19-0224.1.

Neale, R. B., and Coauthors, 2010: Description of the NCAR Community Atmosphere Model (CAM5.0). NCAR Tech. Note NCAR/TN-486+STR, 268 pp., www.cesm.ucar.edu/models/cesm1.1/cam/docs/description/cam5_desc.pdf.

Newman, M., and Coauthors, 2016: The Pacific decadal oscillation, revisited. *J. Climate*, **29**, 4399–4427, https://doi.org/10.1175/JCLI-D-15-0508.1.

Norton, C. W., P.-S. Chu, and T. A. Schroeder, 2011: Projecting changes in future heavy rainfall events for Oahu, Hawaii: A statistical downscaling approach. *J. Geophys. Res.*, **116**, D17110, https://doi.org/10.1029/2011JD015641.

O'Connor, C. F., P.-S. Chu, P. Hsu, and K. Kodama, 2015: Variability of Hawaiian winter rainfall during La Niña events since 1956. *J. Climate*, **28**, 7809–7823, https://doi.org/10.1175/JCLI-D-14-00638.1.

Quan, X.-W., M. P. Hoerling, J. Perlwitz, and H. F. Diaz, 2018: On the time of emergence of tropical width change. *J. Climate*, **31**, 7225–7236, https://doi.org/10.1175/JCLI-D-18-0068.1.

Roeckner, E., and Coauthors, 2003: The atmospheric general circulation model ECHAM5. Part I: Model description. Max Planck Institute for Meteorology Rep. 349, 127 pp., www.mpimet.mpg.de/fileadmin/publikationen/Reports/max_scirep_349.pdf.

Schneider, U., A. Becker, P. Finger, E. Rustemeier, and M. Ziese, 2020: GPCC full data monthly product version 2020 at 0.25°: Monthly land-surface precipitation from rain-gauges built on GTS-based and historical data, DWD, accessed June 2021, https://doi.org/10.5676/DWD_GPCC/FD_M_V2020_025.

Schubert, S. D., M. J. Suarez, P. J. Pegion, R. D. Koster, and J. T. Bacmeister, 2004: On the cause of the 1930s Dust Bowl. *Science*, **33**, 1855–1859, https://doi.org/10.1126/science.1095048.

——, and Coauthors, 2007: Predicting drought on seasonal-to-decadal time scales. *Bull. Amer. Meteor. Soc.*, **88**, 1625–1630, http://ocp.ldeo.columbia.edu/res/div/ocp/pub/schubert/Schubert_etal_2007_BAMS.pdf.

Seager, R., and M. Hoerling, 2014: Atmosphere and ocean origins of North American droughts. *J. Climate*, **27**, 4581–4606, https://doi.org/10.1175/JCLI-D-13-00329.1.

——, Y. Kushnir, C. Herweijer, N. Naik, and J. Velez, 2005: Modeling the tropical forcing of persistent droughts and pluvials over western North America: 1856–2000. *J. Climate*, **18**, 4068–4091, https://doi.org/10.1175/JCLI3522.1.

——, and Coauthors, 2015: Causes of the 2011–2014 California drought. *J. Climate*, **28**, 6997–7024, https://doi.org/10.1175/JCLI-D-14-00860.1.

Serreze, M., and J. Stroeve, 2015: Arctic sea ice trends, variability, and implications for seasonal ice forecasting. *Philos. Trans. Roy. Soc.*, **A373**, 20140159, https://doi.org/10.1098/rsta.2014.0159.

Slivinski, L. C., and Coauthors, 2019: Towards a more reliable historical reanalysis: Improvements for version 3 of the Twentieth Century Reanalysis system. *Quart. J. Roy. Meteor. Soc.*, **145**, 2876–2908, https://doi.org/10.1002/qj.3598.

Sun, L., D. Allured, M. Hoerling, L. Smith, J. Perlwitz, D. Murray, and J. Eischeid, 2018: Drivers of 2016 record Arctic warmth assessed using climate simulations subjected to factual and counterfactual forcing. *Wea. Climate Extremes*, **19**, 1–9, https://doi.org/10.1016/j.wace.2017.11.001.

Taylor, K. E., R. J. Stouffer, and G. A. Meehl, 2012: An overview of CMIP5 and the experiment design. *Bull. Amer. Meteor. Soc.*, **93**, 485–498, https://doi.org/10.1175/BAMS-D-11-00094.1.

Timm, O., and H. F. Diaz, 2009: Synoptic-statistical approach to regional downscaling of IPCC twenty-first-century climate projections: Seasonal rainfall over the Hawaiian Islands. *J. Climate*, **22**, 4261–4280, https://doi.org/10.1175/2009JCLI2833.1.

——, ——, T. W. Giambelluca, and M. Takahashi, 2011: Projection of changes in the frequency of heavy rain events over Hawaii based on leading Pacific climate modes. *J. Geophys. Res.*, **116**, D04109, https://doi.org/10.1029/2010JD014923.

——, S. Li, J. Liu, and D. W. Beilman, 2021: On the changing relationship between North Pacific climate variability and synoptic activity over the Hawaiian Islands. *Int. J. Climatol.*, **41** (Suppl. 1), E1566–E1582, https://doi.org/10.1002/joc.6789.

Zhang, C., Y. Wang, K. Hamilton, and A. Lauer, 2016a: Dynamical downscaling of the climate for the Hawaiian Islands. Part I: Present day. *J. Climate*, **29**, 3027–3048, https://doi.org/10.1175/JCLI-D-15-0432.1.

——, ——, ——, and ——, 2016b: Dynamical downscaling of the climate for the Hawaiian Islands. Part II: Projection for the late twenty-first century. *J. Climate*, **29**, 8333–8354, https://doi.org/10.1175/JCLI-D-16-0038.1.

Zhang, T., M. Hoerling, A. Hoell, J. Perlwitz, and J. Eischeid, 2020: Confirmation for and predictability of distinct U.S. impacts of El Niño flavors. *J. Climate*, **33**, 5971–5991, https://doi.org/10.1175/JCLI-D-19-0802.1.